Proceeding of the IEEE
International Conference on Robotics and Biomimetics
Dali, China, December 2019

Effects of the Varying Lateral Clearances on the Pressure Ripple of Internal Gear Pumps in Biped Robots

Du Ruilong and Yuan Haihui

Intelligent Robot Research Center

Zhejiang Lab
Hangzhou, Zhejiang Province, China
{durl & yuanhh}@zhejianglab.com

Gu J. Jason

Department of Electrical Engineering

Dalhousie University
Halifax, Nova Scotia, Canada
jason.gu@dal.ca

Zhou Hua

State Key Laboratory of Fluid Power & Mechatronic Systems
Zhejiang University
Hangzhou, Zhejiang Province, China
hzhou@sfp.zju.edu.cn

***Abstract* - Internal gear pumps (IGPs) are commonly applied in biped robots' hydraulic actuation systems serving as the power unit. The pump's outlet pressure ripple does harm to accurate motion controls and is usually lowered by adopting an accumulator. This paper investigates the effects of the varying lateral clearances between the gear and the floating plate on the pressure ripple. It aims to provide advices on manufacturing the gears to lower the pump's outlet pressure ripple so that the accumulator could be smaller, which is of great importance to weight and space saving in biped robots' design. A mathematical model was established for evaluating the outlet pressure considering the lateral clearances' varying phenomenon. Moreover, the outlet pressure was measured by high-frequency pressure sensors for verifying the effects of the varying lateral clearances. The simulated and experimental results suggest that the outlet pressure concerning varying lateral clearances has small ripples characterized by high frequency and big ripples characterized by low frequency. Additionally, the pressure ripple, especially the big ripple, can be lowered by well manufacturing the gear pair's lateral sides, ensuring the consistency of the tooth width of the gear.**

***Index Terms* - internal gear pump; pressure ripple; lateral clearance; biped robot.**

I. Introduction

Hydraulic actuation systems are successfully applied in biped robots, for their unique advantages such as compactness and high power-to-weight ratio[1, 2]. A typical hydraulic actuation system is shown in Fig. 1, which mainly consists of a power unit to provide high pressure fluid, some related valves for motion controls and actuators for motions. Usually, the high pressure fluid is provided by a fixed-displacement pump driven by a variable-speed servo motor, and the pressure is regulated by a relief valve.

However, the pump's outlet pressure has ripples, which does harm to accurate motion controls[3, 4]. Thus, an accumulator needs to be adopted to lower the ripples, resulting in un-favored additional weight and structural complexity of the power unit. By well designing and manufacturing the pump, its outlet pressure ripple can be lowered so as to smaller the accumulator, even to cancel the accumulator.

Fig. 2 shows the general configuration of an internal gear pump (IGP), a type of hydraulic pump whose outlet pressure ripple is the lowest[5]. An internal gear pair, comprised of a driving gear shaft and a driven ring gear, is responsible for fluid delivery. A filler is nested within the gear pair for the division of the high pressure area (HP) and the low pressure area (LP). Two floating plates are held tightly against the lateral sides of the gear pair for area sealing, and each floating plate has two sides, the balance side facing away from the gear and the clearance side that faces the gear. Lateral clearances form between the floating plate's clearance side and the gear's lateral side, where thin oil film exists, usually on the magnitude of microns between 0 and 30 μm, leading to a leakage flow from the HP area to the LP area and a consequent increase of the outlet pressure ripple.

Due to manufacturing tolerances, the tooth widths of the gear vary from each other, resulting in varying lateral clearances and a greater outlet pressure ripple. Though it may be negligible by using a bigger accumulator in other engineering practices, it cannot be ignored in biped robots where weight and space saving is of great importance to biped robots' design.

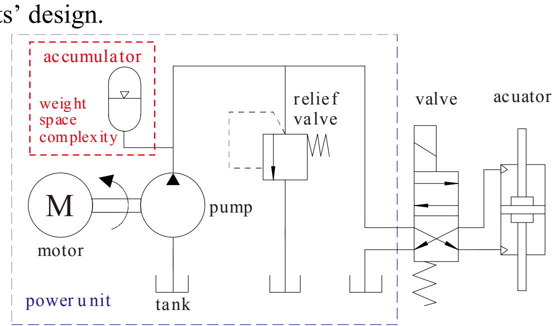

Fig. 1 Schematics of a hydraulic actuation system in biped robots

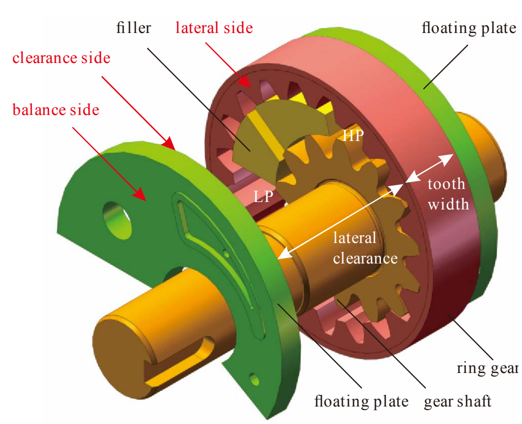

Fig. 2 General configuration of an internal gear pump

Different studies were undertaken to reveal the characteristics of the oil film in the lateral clearance in order to investigate the leakage and the pressure ripples. Hooke et al. calculated the oil film thickness by leveraging formulations of typical lubrication theory, based on the assumption that the oil film was in a certain shape [6, 7]. Borghi et al. analysed the pressure distribution of the oil film so as to evaluate the balance condition of the floating plate using CFD applications [8]. Morgridge et al. proposed a mixed-lubrication model accounting for the influence of the surface roughness [9]. Vacca et al. implemented a fluid structural thermal interaction model to investigate the lubrication behavior of the lateral clearance, especially the impact of the elastic deformation in the gear and the floating plate[10, 11]. Zhou et al. theoretically analysed the pump's outlet flow ripple as well as the pressure ripple, indicating that greater leakage via the lateral clearance tended to increasing the ripple [12]. However, in the previous studies, the lateral clearance was assumed constant, and the varying phenomenon of the lateral clearance, especially due to varying tooth widths induced by manufacturing tolerances, was not taken into account.

After a thorough literature review, few publications could be found on the outlet pressure ripples regarding the varying lateral clearances in IGPs. The goal of this work was to investigate the effects of the varying lateral clearances on the outlet pressure ripples in IGPs. In the present work, a mathematical model was established for the evaluation of the outlet pressure considering the lateral clearances' varying phenomenon. Additionally, a test rig was built to measure the outlet pressure of an IGP for verifying the effects of the varying lateral clearances.

II. Mathematical Model

Fig. 3 depicts the pressure areas divided by the filler nested within the internal gear pair. It can be seen that the gear shaft (driving gear) which has 13 teeth is eccentric with the ring gear (driven gear) which has 19 teeth, and the meshing point travels along the meshing line (the blue line). By meshing the gears, fluid is sucked into the LP area due to the volume increase of the LP area, delivered to the HP area as the gear rotates, and discharged out of the HP area due to the volume decrease of the HP area. As observed, the fluid pressure of the HP area corresponds to the pump's outlet pressure.

Fig. 4 depicts the hydraulic system for modelling the IGP's outlet pressure. In order to minimum the uncertain factors introduced by other hydraulic components such as valves, to improve the accuracy level of the simulation model, a simple hydraulic system is adopted. In the system, an orifice serves as the purpose of building up the pump's pressure, and a delivery pipe with a constant diameter is utilized as the connection between the pump's outlet and the orifice. The outlet pressure with respect to time can be evaluated by applying the mass conservation equation, as shown in (1).

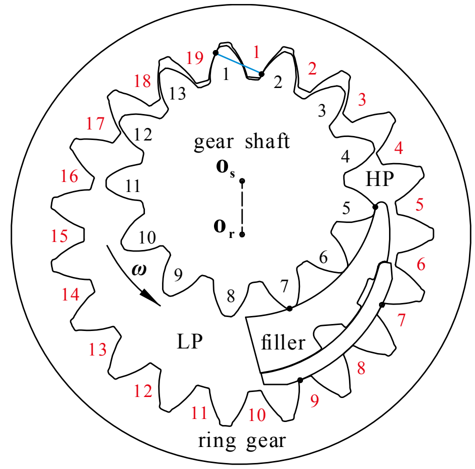

Fig. 3 Pressure areas divided by filler nested within the internal gear pair

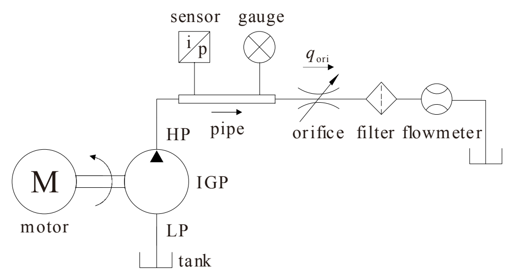

Fig. 4 Schematics of the hydraulic system for modelling the IGP's outlet pressure

$$\frac{\mathrm{d}p}{\mathrm{d}t} = \frac{\beta}{V}\left(\sum q_{\text{in}} - \sum q_{\text{out}} - \frac{\mathrm{d}V}{\mathrm{d}t}\right) \tag{1}$$

In (1), β represents the fluid bulk modulus; V represents the volume of the HP area and the delivery pipe; $\mathrm{d}V/\mathrm{d}t$ represents the time derivative of the area's volume; q_{in} and q_{out} represent the flow into and out of the area. Detailed expressions for the terms above were presented in [5] except for the lateral leakage via the lateral clearance between the floating plate's clearance side and the gear's lateral side.

Fig. 5 depicts the lateral leakages via the lateral clearances between the floating plates and the gear pair. It can be seen that two sealing areas are formed: one by the ring gear and the floating plate, and the other by the gear shaft and the floating plate. Due to the complexity of the gear geometry, the lateral leakage for one tooth can be approximated using (2).

$$q_{\text{j}} = \frac{b \cdot \delta_{\text{j}}^{3}}{12\mu \cdot \left(r_{\text{p}} - r_{\text{fp}}\right)} p \tag{2}$$

In (2), μ represents the viscosity of the fluid; δ_{j} represents the clearance between the tooth's lateral side and the floating plate's clearance side. It should be noted that δ_{j} for each tooth is different since the tooth width varies. For the gear shaft's teeth, δ_{j} varies between 20 and 30 μm; for the ring gear's teeth, δ_{j} varies between 20 and 35 μm.

After obtaining the detailed expressions for the terms in the right-hand side of (1), it can be found that the right-hand side of (1) is an equation of pressure (p) and time (t).

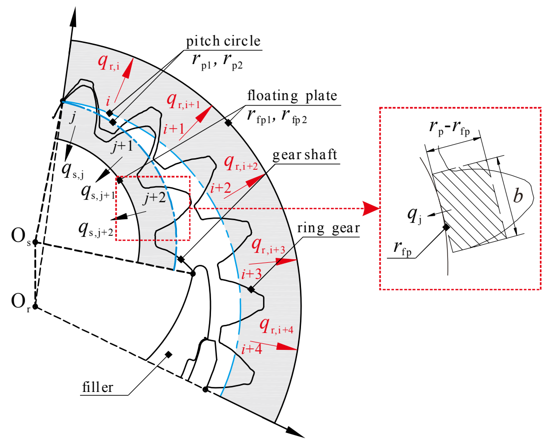

Fig. 5 Leakages via the lateral clearances between the floating plates and the gear pair

Hence, (1) can be written as a differential equation as shown in (3).

$$\frac{\mathrm{d}\,p}{\mathrm{d}\,t}=f\left(p,t\right) \tag{3}$$

Equation (3) can be solved numerically be leveraging the fourth-order Runge-Kutta method (RK4). Details of the algorithm scheme was presented in [12], except for the criteria for the convergence of the simulation. It is clear that the gear shaft's tooth will mesh the same tooth of the ring gear after 247 meshing periods (13*19) because the gear shaft has 13 teeth and the ring gear has 19 teeth. Therefore, the 247 meshing periods were referred to as a cycle, and at the end cycle, the outlet pressure in one cycle served as the criteria to judge the convergence of the simulation using (4).

$$\sum\left|p_{\mathrm{new}}-p_{\mathrm{old}}\right|/\sum\left|p_{\mathrm{new}}\right|\leq p_{\mathrm{err}} \tag{4}$$

In (4), p_{new} represents the pressure in the present cycle; p_{old} presents the pressure the previous cycle; p_{err} represents the error between the pressure in the two successive cycles (converged to 10^{-8}).

III. Analysis and Discussion

In order to investigate the effects of the varying phenomenon of the lateral clearances, a comparison was made between the gears with the same tooth width (flatness) and the gears with different tooth widths (non-flatness). As concerns the case of flatness, the lateral clearance was constant and was set 20 µm. As concerns the case of non-flatness, the lateral clearances varied; regarding the gear shaft, they were set between 20 and 30 µm; regarding the ring gear, they were set between 20 and 35 µm. Moreover, it should be noted that the varying lateral clearances subjected to Gaussian distribution, which was in accordance with the manufacturing process.

Fig. 6 depicts the simulated outlet pressure ripples regarding the cases of flatness and non-flatness, 3000 rpm, 7 MPa. As observed in Fig. 6 (a), the time span is 0.2 s, indicating that the gear shaft has rotated for 10 revolutions, 130 meshing periods. The pressure concerning the case of flatness (in red line) repeats itself every one meshing period, while that concerning the case of non-flatness (in blue line) repeats itself every 247 meshing periods, suggesting that the non-flatness results in a more complex pressure ripple. Additionally, the pressure of flatness varies between 7.26 and 7.45 MPa, while that of non-flatness varies between 6.45 and 7.51 MPa, approximately six times that of flatness, suggesting that the non-flatness results in a greater pressure ripple. This is mainly because the lateral clearances of non-flatness are generally greater than those of flatness, leading to a greater lateral leakage which is proportional to the cube of the lateral clearance as shown in (2). Apart from that, it suggests that greater leakage tends to increase the pressure ripple, which is consistent with [12].

Referring to Fig. 6 (b), the time span is 0.02 s, indicating that the gear shaft has rotated for one revolution, 13 meshing periods. It can be seen that the pressure of non-flatness (in solid blue line) shows a big ripple globally, as outlined by the dotted blue line. Moreover, 13 local small ripples can be seen accompanying with the global big ripple, consistent with the gear shaft's tooth number (13). As concerns the pressure of flatness (in red line), there exist 13 small ripples and no big ripples. Hence, it suggests that the pressure ripples of non-flatness are composed of big ripples and small ripples, while the pressure ripples of flatness are composed of small ripples.

Fig. 7 depicts the frequency spectrum of the outlet pressure ripples, 3000 rpm, 7 MPa. As concerns the frequency spectrum of flatness (in red line), the base frequency is 650 Hz (f_0) with an amplitude of 0.008 MPa, which is consistent with the small ripples in Fig. 6, mainly determined by the tooth number and the rotation speed of the gear shaft as shown in (5). Moreover, since the pump usually operates above 1500 rpm, it can be seen that the small ripples are generally characterized by high frequency. Apart from that, it is worth noting that the amplitudes of frequency spectrum are zero except for the base frequency and its multiples.

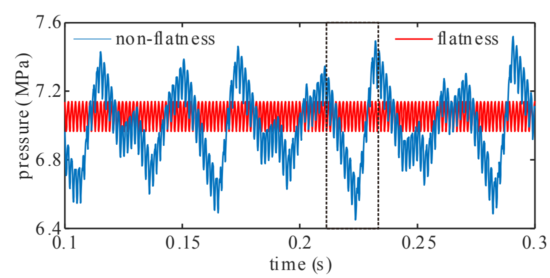

(a) pressure ripple for 0.2 s

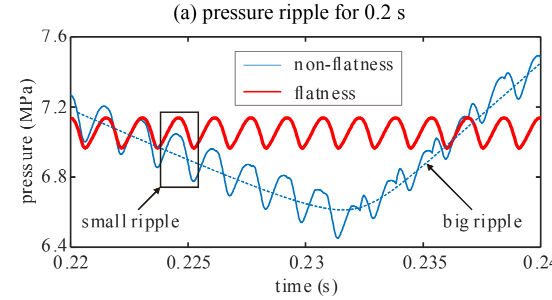

(b) pressure ripple for 0.02 s

Fig. 6 Outlet pressure ripples regarding the cases of flatness and non-flatness, 3000 rpm, 7 MPa

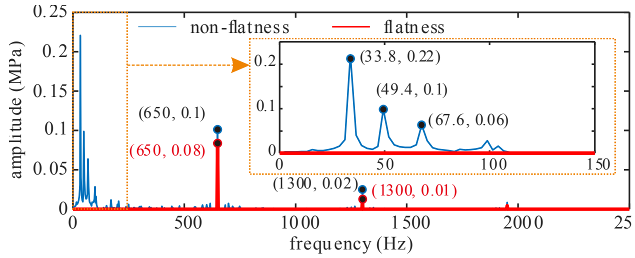

Fig. 7 Frequency spectrum of the outlet pressure ripples, 3000 rpm, 7 MPa

$$f_0 = z_1 n / 60 \tag{5}$$

With respect to the frequency spectrum of non-flatness (in blue line), it can be seen that there exists a peak amplitude for the base frequency of f_0 and its multiples, and the amplitude is greater than that of flatness, suggesting a greater ripple of non-flatness. Moreover, peak amplitudes can be observed at the region of low frequency, which mainly appear at the frequencies of 33.8 Hz (f_r), 49.4 Hz (f_s) and the multiples of f_r and f_s. Judging from Fig. 6 and Fig. 7, the region of low frequency can be seen consistent with the big ripples in Fig. 6, and the frequencies of f_r and f_s are mainly determined by the gear pair's tooth numbers and the gear shaft's rotation speed as shown in (6) and (7). It suggests that the big ripples are generally characterized by low frequency.

Since the control frequency of the valves in biped robots is generally lower than 200 Hz, lowering the ripples at the region of low frequency is of great importance to accurate motion controls, thus making the accumulator smaller. It could be accomplished by well manufacturing the gear's lateral sides, improving the lateral clearances' consistency. Additionally, it is worthwhile to note that the amplitudes concerning f_r are greater than those concerning f_s, and this is because the lateral clearances concerning the ring gear are generally greater, leading to a greater leakage than that concerning the gear shaft. Hence, it suggests that the consistency of the tooth width should be checked in both the gear shaft and the ring gear, not just only in the gear shaft or in the ring gear.

$$f_r = z_1 n / (60 \cdot z_2) \tag{6}$$

$$f_s = n / 60 \tag{7}$$

Fig. 8 depicts the frequency spectrum of the outlet pressure ripples for 2000 rpm and 1000 rpm, 7MPa, non-flatness. It is clear that the phenomena displayed in Fig. 8 are consistent with those describe above in Fig. 7. Apart from that, greater amplitudes can be observed at the region of low frequency as the rotation speed decreases, suggesting that big ripples become more noticeable under low rotation speeds.

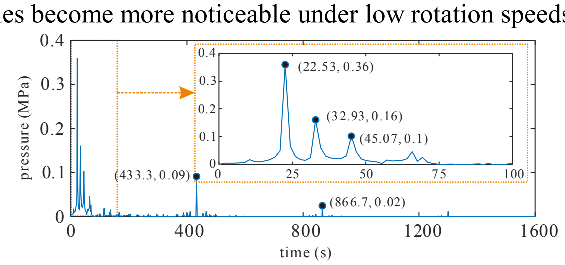

(a) 2000 rpm

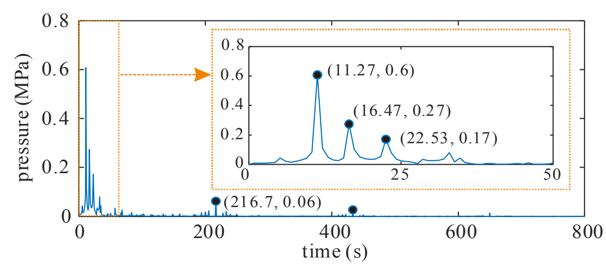

(b) 1000 rpm

Fig. 8 Frequency spectrum of the outlet pressure ripples for 2000 rpm and 1000 rpm, 7 MPa, non-flatness

IV. Experiments

In order to verify the effects of the varying lateral clearances, a test rig was set up for measuring the outlet pressure of the IGPs as depicted in Fig. 9. It should be underlined that the layout of test rig was in accordance with the hydraulic schematics as depicted in Fig. 4. The IGP was driven by a motor (0-3000 rpm), and the pump's outlet was connected to a straight pipe with a constant diameter. An orifice was installed at the other end of the pipe for the purpose of building up the pump's outlet pressure. A 100 KHz pressure sensor, whose measuring scale was 0-35 MPa with 0.5% accuracy and 0.5% nonlinearity, was installed at the outlet of the pump for capturing the outlet pressure ripples.

Fig. 10 depicts the measured tooth widths of the gear shaft and the ring gear using a micrometer. The tooth widths of the gear shaft vary between 15.505 and 15.535 mm; the tooth widths of the ring gear vary between 15.480 and 15.505 mm. Since the floating plates are held tightly against the lateral sides of the gear pair, it suggests that the lateral clearances between the ring gear and the floating plate are generally greater than those between the gear shaft and the floating plate.

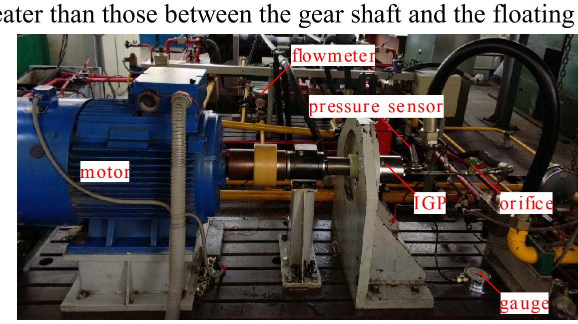

Fig. 9 Test rig for measuring the outlet pressure ripples of the IGP

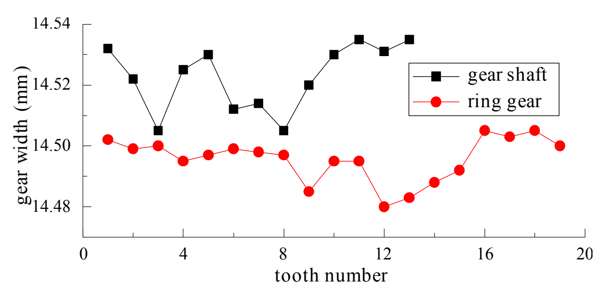

Fig. 10 Tooth widths of the gear shaft and the ring gear

Fig. 11 depicts the frequency spectrum of the measured outlet pressure ripples, 3000 rpm, 7 MPa. As observed in Fig. 11 (a), there exist peak amplitudes at the base frequency of 642 Hz (f_0) and its multiples, which corresponds to the small ripples of the outlet pressure and is consistent with the analysis above as shown in (5).

Referring to Fig. 11 (b), at the region of low frequency, peak amplitudes occur at the frequencies of 34 Hz (f_r), 49 Hz (f_s) and their multiples, which corresponds to the big ripple and is consistent with (6) and (7) as analysed above. Apart from that, the amplitudes concerning f_r can be observed greater than those concerning f_s. This is mainly because the lateral clearances between the ring gear and the floating are greater, thus leading to a greater leakage than that concerning the gear shaft. It can be seen that this is also consistent with the analysis above on the consistency check in tooth widths.

V. Conclusions

This paper discusses the effects of the varying lateral clearances on the outlet pressure ripples of internal gear pumps in biped robots. Judging from the simulated and experimental results, several conclusions may be drawn as follows.

(1) Regarding the case of constant lateral clearance, the outlet pressure ripples only have small ripples characterized by high frequency, whose base frequency is mainly determined by the tooth number and the rotation speed of the gear shaft.

(2) Regarding the case of varying lateral clearances, the outlet pressure ripples have big ripples characterized by low frequency and small ripples characterized by high frequency. The base frequencies of the big ripples are mainly determined by the gear pair's tooth numbers and the gear shaft's rotation speed.

(3) The pressure ripples, especially the big ripples characterized by low frequency, do harm to accurate motion controls in biped robots. The pressure ripples, especially the big ripples, can be lowered by well manufacturing the gear pair, ensuring the consistency of the tooth widths of the gear.

(4) The consistency of the tooth widths should be checked in both the gear shaft and the ring gear, not just only in the gear shaft or in the ring gear.

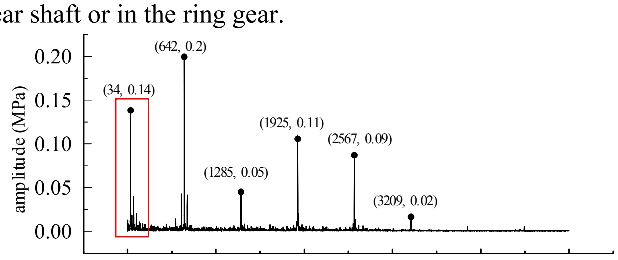

(a) spectrum between 0 and 5000 Hz

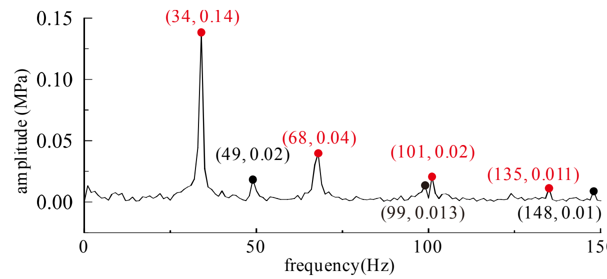

(b) spectrum at the region of low frequency

Fig. 11 Frequency spectrum of the measured outlet pressure ripples, 3000 rpm, 7 MPa

References

[1] G. Nelson, A. Sauders and R. Playter, "The PETMAN and Atlas robots at Boston Dynamics," *Humanoid Robotics*, pp. 169-186, 2019.

[2] Y. Lei, J. Luo, C. Fu, J. W and Y. Fu. "Mechanical design and gait plan of a hydraulic-actuated biped robot," in *2015 IEEE International Conference on Mechatronics and Automation (ICMA)*, Beijing, China, pp.1132-1137.

[3] S. Ye, J. Zhang, B. Xu, S. Zhu, J. Xiang and H. Tang, "Theoretical investigation of the contributions of the excitation forces to the vibration of an axial piston pump," *Mechanical Systems and Signal Processing*, vol. 129, pp. 201-217, 2019.

[4] J. Zhang, S. Xia, S. Ye, B. Xu, W. Song, S. Zhu, et al. "Experimental investigation on the noise reduction of an axial piston pump using free-layer damping material treatment," *Applied Acoustics*, vol. 139, pp. 1-7, 2018.

[5] R. Du, Y. Chen and H. Zhou. "Numerical analysis of the lubricating gap between the gear shaft and the journal bearing in water hydraulic internal gear pumps," *Proceedings of the Institution of Mechanical Engineers, Part C: Journal of Mechanical Engineering Science*, vol.232, No.12, pp. 2297-2314, 2018.

[6] C. J. Hooke and E. Koc. "End plate balance in gear pumps," *Proceedings of the Institution of Mechanical Engineers, Part B: Management and engineering manufacture*, vol. 198, No. 1, pp. 55-60, 1984.

[7] E. Koc, "An investigation into the performance of hydrostatically loaded end-plates in high pressure pumps and motors: movable plate design," *Wear*, vol. 141, No. 2, pp. 249-265, 1991.

[8] M. Borghi, M. Milani, F. Paltrinieri and B. Zardin, "Studying the axial balance of external gear pumps," *SAE Technical Paper*, pp. 2005-01-3634, 2005.

[9] D. Morgridge, H. P. Evans, R. W. Snidle and M. K. Yates, "A study of seal lubrication in an aerospace fuel gear pump including the effects of roughness and mixed lubrication," *Tribology Transactions*, vol. 54, No. 4, pp. 657-665, 2011.

[10] D. Thiagarajan and A. Vacca, "Mixed lubrication effects in the lateral lubricating interfaces of external gear machines: modelling and experimental validation," *Energies*, vol. 10, No. 1, pp. 111, 2017.

[11] D. Thiagarajan, S. Dhar and A. Vacca, "A novel fluid structure interaction-ehd model and optimization procedure for an asymmetrical axially balanced external gear machine," *Tribology Transactions*, vol. 58, No. 2, pp. 274-287, 2015.

[12] H. Zhou, R. Du, A. Xie and H. Yang. "Theoretical analysis for the flow ripple of a tandem crescent pump with index angles," *Applied Sciences*, vol. 7, No. 11, pp. 1148, 2017.